Citation:
Ghaffari, S (2023) Sustainable crumb rubber modified asphalt mixtures based on low-temperature crack propagation characteristics using the response surface methodology. Theoretical and Applied Fracture Mechanics, 123. ISSN 0167-8442 DOI: https://doi.org/10.1016/j.tafmec.2022.103718

Link to Leeds Beckett Repository record:
https://eprints.leedsbeckett.ac.uk/id/eprint/9186/

Document Version:
Article (Published Version)

Creative Commons: Attribution 4.0

© 2022 The Author(s).

The aim of the Leeds Beckett Repository is to provide open access to our research, as required by funder policies and permitted by publishers and copyright law.

The Leeds Beckett repository holds a wide range of publications, each of which has been checked for copyright and the relevant embargo period has been applied by the Research Services team.

We operate on a standard take-down policy. If you are the author or publisher of an output and you would like it removed from the repository, please contact us and we will investigate on a case-by-case basis.

Each thesis in the repository has been cleared where necessary by the author for third party copyright. If you would like a thesis to be removed from the repository or believe there is an issue with copyright, please contact us on openaccess@leedsbeckett.ac.uk and we will investigate on a case-by-case basis.

Theoretical and Applied Fracture Mechanics 123 (2023) 103718

Contents lists available at ScienceDirect

Theoretical and Applied Fracture Mechanics

journal homepage: www.elsevier.com/locate/tafmec

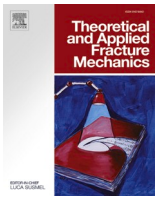

Sustainable crumb rubber modified asphalt mixtures based on low-temperature crack propagation characteristics using the response surface methodology

Sepehr Ghafari [a,*], Sajad Ranjbar [b], Mehrdad Ehsani [b], Fereidoon Moghadas Nejad [b], Parneet Paul [a]

[a] School of Built Environment, Engineering and Computing, Leeds Beckett University, United Kingdom
[b] Department of Civil & Environmental Engineering, Amirkabir University of Technology (Tehran polytechnic), Iran

ARTICLE INFO

Keywords:
Sustainable Optimization
Low-Temperature Fracture
Asphalt Concrete
Crumb Rubber
Response Surface Methodology

ABSTRACT

Fracture regime of asphalt concrete is of utmost importance in the sustainable design of optimized mixtures against low-temperature cracking. The energy dissipated in blunting the crack tip, stable crack growth, as well as post-peak resistance of the mixtures to the propagating crack comprise the overall fracture performance of the mixtures. In this research, employing the fracture resistance curve (R-curve) concept, three energy parameters: cohesive energy, fracture energy, and energy rate, are extracted to quantify the crack propagation regime of the mixtures incorporating ground recycled waste tire. A temperature range of 0 °C to −20 °C with 0 %, 10 %, and 20 % crumb rubber contents (CRC) were considered and the experiments were carried out in Single Edge notched Beam (SE(B)) fracture testing protocol. An environmental index comprising CO_2 and CH_4 emissions, as well as the energy consumption, was developed and the production cost of AC samples were also determined. A design of experiments based on the Central Composite Design (CCD) is applied. The Response Surface Methodology (RSM) is used to develop the best model between the fracture response, environmental factor, cost, and the input mixture properties. Multi-objective optimization scenarios were assessed by the RSM and a 4.74 % binder content with 19.5 % crumb rubber incorporation was resulted as the optimal mix design for maximum fracture response and minimized cost and environmental concerns in low temperatures. The environmental effects and costs were by average reduced by 15 % and 1 %, respectively and fracture responses have been improved compared to the reference optimum mix design (CRC = 0).

1. Introduction

Mechanical performance of the asphalt concrete must come under close scrutiny when optimizing mixtures for low-temperature cracking considering environmental and economic aspects to tackle the risk of mid-term to long-term distress occurrence in pavement structures. Transverse cracks with a spacing of 1 m to 30 m [1] perpendicular to the direction of traffic are pertinent to the fracture of the asphalt layers in pavements at low temperatures impacting a sustainable approach to design. Thus, a comprehensive low-temperature fracture characterization of asphalt concrete (AC) and bituminous mixtures has been a topic of vital interest for researchers of sustainable engineering materials for the past two decades.

Among the earliest endeavors in applying fracture mechanics concepts in the characterization of AC behavior at low temperatures, Kim and El Hossein [2] determined the fracture toughness (K_{IC}) values of AC mixtures. They used a linear elastic approach and investigated the effect of temperature reduction on the fracture toughness of AC. The fracture toughness exhibited a rise as the temperature was reduced from −5 °C to −15 °C while it dropped at lower temperatures due to internal damage in the mixtures. This approach has been widely used to characterize modified and unmodified AC mixtures to date [3–5]. An investigation was accomplished by Li and Marasteanu [6] in 2010 utilizing the acoustic emissions in a semi-circular bend (SC(B)) fracture test to capture the size of the fracture process zone (FPZ) ahead of the crack tip in AC. It was observed that the FPZ of hot mix asphalt (HMA) has a significant size in intermediate to low temperatures. The findings of this research were later confirmed by Doll et al. [7], where the digital image

* Corresponding author.
E-mail address: s.ghafari@leedsbeckett.ac.uk (S. Ghafari).

https://doi.org/10.1016/j.tafmec.2022.103718
Received 6 June 2022; Received in revised form 4 December 2022; Accepted 5 December 2022
Available online 10 December 2022
0167-8442/© 2022 The Author(s). Published by Elsevier Ltd. This is an open access article under the CC BY license (http://creativecommons.org/licenses/by/4.0/).

correlation (DIC) technique was applied to study the size of the FPZ in AC mixtures. The large size of the FPZ at low temperatures and the nonlinear and inelastic behavior of bituminous mixtures could necessitate caution in applying the classical stress intensity factor concepts in characterizing the stress fields in the crack tip in bituminous materials. Hence, for the past decade, considerable research has focused on the characterization of the mixtures through other fracture concepts such as the J-integral, C* integral, and fracture energy [8–10]. Amongst the parameters mentioned above, the fracture energy began to gain considerable attention leading to the establishment of codes such as ASTM D7313-20 and AASHTO TP105-20 based on the disc-shaped compact tension test and the semi-circular test protocols. The fracture energy reported potentially consists of various components, such as the energy required to initiate the crack, the energy to advance the crack, and viscous dissipations [11]. Fracture resistance curves (R-curves) are a well-established fracture concept for a comprehensive characterization of the crack propagation regime of engineering materials [12,13]. R-curves could be used as a complementary tool in addition to the fracture energy to distinguish between the work required to initiate the crack and the energy for the propagation of the crack while addressing the stable crack growth phase and initiation of unstable crack growth. R-curves have been widely used in fracture analysis of engineering materials such as wood [14], ceramics [15], concrete [12], etc. However, experimental costs and difficulties have substantially restricted their use in characterizing bituminous mixtures. Ghafari and Nejad [16,17] determined low-temperature J-Resistance curves of AC mixtures by conducting SE (B) tests on various mixtures and processing captured images during each test. Critical values such as the fracture initiation toughness (J_{IC}), and the fracture instability toughness (J_{inst}) in relation to the critical crack length triggering the unstable crack propagation were determined. Yang and Braham [18] derived R-curves of various AC mixtures in terms of cumulative fracture energy as a function of crack length. They proposed three parameters: fracture energy, cohesive energy, and fracture rate to characterize the mixtures' fracture trend. These parameters can give a broader inference of the fracture trend of the mixtures at low temperatures. Crumb rubber modified bitumen with warm mix technology was used in a research by Wang and Liu [19] to assess the fatigue performance of the mixtures. It was found that the rubberized bitumen exhibited superior performance in terms of long-term fatigue than the neat bitumen. Regarding fracture performance, the 20 % crumb rubber modified mixtures showed greater fracture toughness magnitudes in mode I and mixed-mode (I/II) cracking in a study by Razmi and Mirsayar [20]. It was also revealed in a recent study by Ghafari and Nejad [21] that, the stable crack growth phase in mixed-mode (I/II) R-curves of crumb rubber modified AC mixtures is significantly enlarged leading to higher energy dissipations to advance the crack tip. J-resistance curves for crumb rubber modified mixtures were determined using an experimental J-integral calculation approach by Ghafari and Nejad [22]. It was revealed in their research that the crumb rubber modification induces further energy dissipations in the mixtures to advance the crack tip as well as enlarging the size of the stable crack growth zone. In another research, the fracture properties of AC mixtures having crumb rubber were investigated by Chen and Solaimanian [23] using the linear amplitude sweep test and the Glover-Rowe (G-R) parameter derived from dynamic shear rheometer (DSR). The flexibility and crack resistance of the crumb rubber modified mixtures were greater than the unmodified mixtures.

Economic and social development is in direct relationship with transportation infrastructure. Therefore, most countries are putting serious effort into the construction of new roadways in addition to improving the quality of construction [24]. Pavements serve as the structure of the roadways, and flexible pavements are approximately the most common type of pavements. The highway network in the United States consists of 4.3 million kilometers of roadways, 94 % of which being flexible pavement systems [25]. In other words, 3.68 million kilometers of the roadways in the United States are surfaced by asphalt concrete which is substantially large [26]. Hanson et al. [27] showed that an enormous amount of CO_2 and CH_4 is emitted due to the preparation of the materials used to produce asphalt concrete. The reduction of greenhouse gases could tangibly contribute to the preservation of the environment. Complying with a sustainability approach to design of transportation infrastructures, the influential and multi-aspectual role of pavement structures must be considered [28]. The transportation industry also serves as a fundamental cause of air pollution. According to Mallick and Veeraragavan [29], 30 percent of the global air pollution and 25 percent of fossil fuel consumption is related to this industry, 7 percent of which is allocated to the pavements [30]. Regarding the high impact of such infrastructure on the environment, sustainability has gained increasing global attention in the pavement industry [31]. Several definitions exist on sustainability, which all converge in economic improvements in line with reducing environmental pollutions in decision making [32]. Consequently, simultaneous consideration of economic and environmental factors appears crucial while designing pavements that can reduce carbon emissions, energy, and costs.

Incorporation of crumb rubber derived from waste tire could significantly contribute to the abovementioned goals and fundamentals of the circular economy, the three Rs: Reduce, reuse, and recycling in the construction environment. Carbon emissions reduction by using crumb rubber is proved and emphasized as a measure of waste tire sustainable management [33] while providing an environmentally friendly construction approach [34].

Pavement condition has a substantial impact on road safety and efficiency, and mixture design parameters are one of the most important factors that affect pavement performance in service life [35]. Regarding the benefits and challenges of crumb rubber modification of the AC mixtures and the detailed insight into the fracture regime of the mixtures provided by the R-curves, optimization of the mixtures gains crucial importance. In recent years, the response surface methodology (RSM) has been widely used as a robust tool in modeling and optimizing the asphalt pavement mixtures considering multiple influential factors and the engineering responses [36]. RSM is a statistical method used to evaluate the relation between the considered input factors and experiment responses. In this method, the best model is developed to determine the behavior of experiment response versus the changes in the input factors. After extracting the behavioral model of the experiment, various optimization scenarios can be evaluated in RSM process[37]. The evaluation of the effects of various factors on fractural properties as important responses of asphalt mixture using RSM gets more attention from the research community. Omranian et al.[38] applied RSM to determine the effect of various short-term aging scenarios on fracture properties of the asphalt mixture, such as stress intensity factor, broken aggregate, and adhesion failure. Yıldırım and Karacasu [39] used RSM to evaluate the effect of temperature, waste rubber, glass fiber, and bitumen content on hot mix asphalt performance parameters, including practical specific gravity voids, voids filled with asphalt cement and Marshall stability. Saha and Biligiri [40] assessed the cracking performance of asphalt mixtures in semi-circular bending tests using RSM, considering the air void, asphalt content, thickness, and temperature effects. Rafiq et al. [41] used RSM to analyze and optimize the impact of different percentages of recycled asphalt pavement and crude palm oil on stability, flow, stiffness, mixture voids, voids filled with asphalt, and the indirect tensile strength.

As was elaborated, R-curve characterization of AC, even though providing a detailed insight into the entire fracture regime of the mixtures, has been scarcely conducted in the literature due to experimental costs and difficulties. Moreover, in this fashion, the majority of research to date have conducted asphalt concrete mixture optimization using critical or ultimate fracture parameters [4,42]. Thus, an optimization scheme that accounts for the entire fracture process of the mixtures (crack blunting, initiation, unstable crack propagation, fracture failure) can result in further inclusive outcomes. Hence, in this research, SE(B) fracture testing of crumb rubber modified and unmodified AC mixtures

is conducted in three temperature levels of 0 °C, −10 °C, and −20 °C. 10 % and 20 % crumb rubber addition by weight of the binder is considered in the mixtures using a 3 % warm mix additive (Sasobit). With two gradations, AC mixtures were fabricated by limestone and siliceous aggregate with 4 %, 4.5 %, and 5 % binder content. Crack lengths were obtained by analyzing the captured images during the tests, and the R-curves of the mixtures could be determined. The three parameters: cohesive energy, fracture energy, and energy rate, were extracted from each R-curve, and the RSM was applied to develop three prediction models for the R-curve parameters proceeded by and assessment and verification of the performance of the models in predicting the experimental responses.

Finally, a multi-objective optimization process was employed to optimize mixture proportions considering the three R-curve-driven fracture indices and environmental and cost factors in five target functions. The optimized sustainable mixture design is reported as the outcome of the study.

2. Objective

This study aims to develop a sustainably optimized asphalt concrete mixture design based on low-temperature crack propagation trend as well as cost and environmental factors in pavement engineering problems. Using the three R-curve driven parameters for optimization will not only result in mixtures with optimized resistance to macro-crack initiation but also will select the most desirable mixture in terms of resistance against the propagating crack (in the post-peak phase) which is a key fracture property of the mixture during the service life in pavement layers. The research framework is presented in Fig. 1.

3. Materials and methods

3.1. Materials

Two types of aggregate were used in the mixtures for this research. Limestone aggregate was delivered from an asphalt production plant located west of Tehran, and crushed in a vertical shaft impact crusher. Siliceous aggregate was obtained from a local river bed resource located south of Tehran. The physical properties of the two types of aggregates are presented in Table 1.

The base binder in producing the mixtures was a PG58-22 bitumen. Rheological properties of the bitumen are reported in Table 2. Two different gradations were used to develop AC mixtures specified by the different nominal maximum aggregate size (NMAS) values of 19 mm and 25 mm. Gradation curves are depicted in Fig. 1(a). Based on the Marshall method, the optimum binder content was obtained to be 4.3 % (with NMAS 19 mm) and 4.5 % (NMAS 25 mm) for the mixtures with limestone aggregate and 4.5 % and 4.8 % for the mixtures with siliceous

Table 1
Physical properties of the limestone and siliceous aggregates.

Property	Standard	Limestone aggregate	Siliceous aggregate
LA Abrasion loss	AASHTO T96-02	20	19
Fractured in one face	ASTM D5821-13	>98	>87
Fracture in two faces	ASTM D5821-13	>98	93
Flakiness	BS 812–103.1	5	20
Coating of aggregate	AASHTO T184	98	95
Sodium Solphate loss	AASHTO T104-99	1.8 (fines) 0.7 (coarse)	2.8 (fines) 0.4 (coarse)

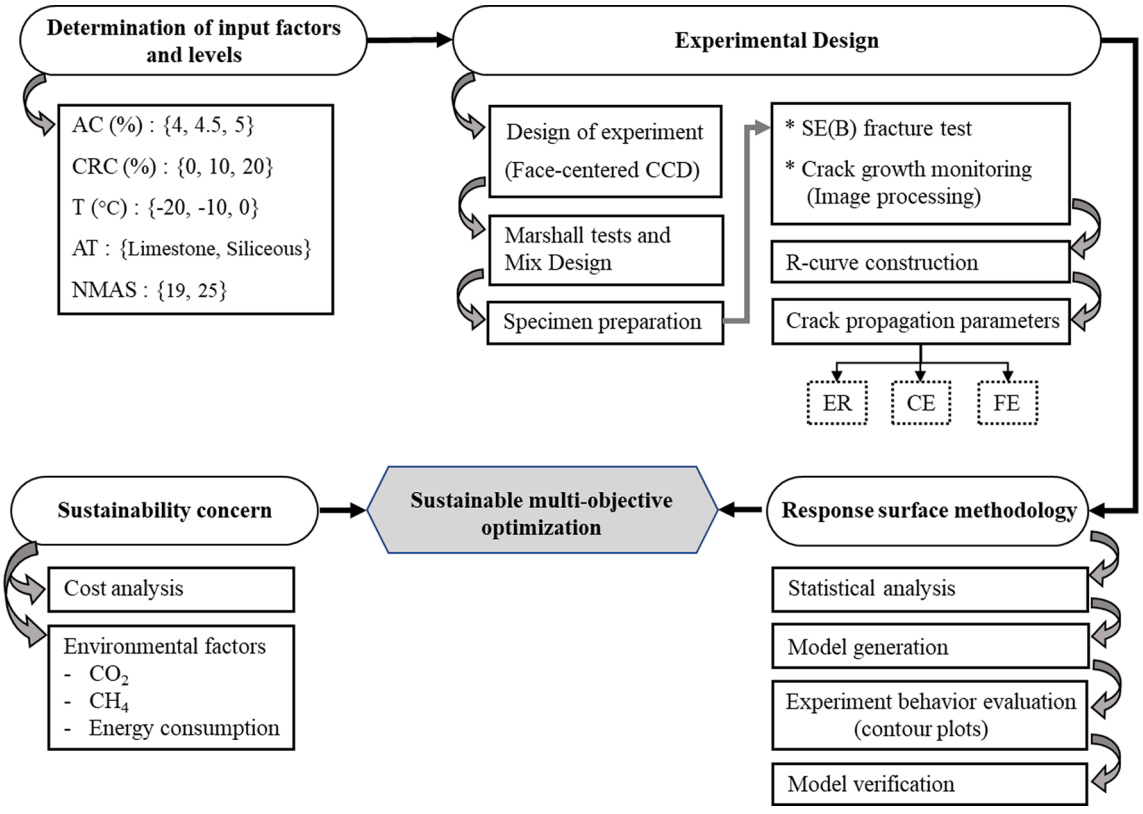

Fig. 1. The research framework.

Table 2
Rheological properties of the base binders.

Property	PG58-22	Test Method
Penetration at 25 °C, 0.1 mm	89	ASTM D5
Softening point (°C)	50.8	ASTM D36
Ductility (15 °C, cm)	>100	ASTM D113
Flashing point (°C)	290	ASTM D92
Density	1.02	ASTM D70
Kinematic viscosity (Centistoke, 120 °C)	790	ASTM D2170
Kinematic viscosity (Centistoke, 135 °C)	370	ASTM D2170
Kinematic viscosity (Centistoke, 160 °C)	130	ASTM D2170
DSR (G*/sin(δ), kPa)	1.29	ASTM D7175

aggregate. Thus, mixtures with 4 %, 4.5 %, and 5 % binder were developed to ascertain including the effect of binder content variation on the low-temperature fracture indices determined in this work.

In this research, crumb rubber powder is prepared by grinding waste tires to a particle size of 0.6 mm (#30), as shown in Fig. 2(b). Crumb rubber modified mixtures were developed, incorporating 10 % and 20 % crumb rubber powder (by weight of the binder) into the mixtures in a wet process. Significant enhancements in rheological characteristics and mechanical performance of rubberized asphalt mixtures have been reported so far [43,44] depending on the process used to incorporate crumb rubber in the mixtures.

Mixing efficiency and the consistency of the resulting binder, high viscosity of the rubberized bitumen, pump-ability, and high energy consumption in the production plants are among the concerns [45] of producing rubberized asphalt mixtures. Warm mix technology has contributed to tackling such issues mainly by reducing the viscosity of the bitumen [46]. Therefore, in the first step, 3 % warm mix additive (Sasobit) by weight of the base binder was mixed with the bitumen at 160 °C by a high-shear rotational mixer at a rotational velocity of 6000 rpm. A mixing time of 15 min was considered. Next, raising the temperature to 180 °C, the crumb rubber powder was mixed with the bitumen for 30 min at a rotational velocity of 2000 rpm resulting in the desired homogeneity of the modified binder. The aggregate was proportioned and heated in the oven to a temperature of 180 °C for at least 4 h prior to the final mixing. Finally, the aggregate and the modified bitumen were mixed at 180 °C, poured into slab molds, and compacted at 170 °C.

Proceeded by a minimum of 7-hour cooling time, the AC slabs were demolded and cut by an automated water-cooled saw to fabricate beam specimens. While no standard is present for SE(B) testing of AC specimens, various research [47,48] is conducted in compliance with ASTM E1820-20b instructions. Beams were initially cut to an overall length of 380 mm, where a 15 mm free margin was considered at each side. Finally, and based on the instructions above, a span length of 320 mm, a height of 80 mm, and a thickness of 40 mm were chosen in this research for the AC beams. The mid-span notch was fabricated targeting a total notch height to width ratio (a/w) of 0.2 [47]. The first 8 mm of the notch length was cut to a width of 5 mm by the automated saw. The remaining 8 mm was cut using a handsaw to a maximum width of 1 mm. The AC beam specimen dimensions and the notch length is depicted in Fig. 3. A water-based white paint was applied on the two sides of each beam in order to induce desirable contrast for tracking the crack length across the beam surface when analyzing the digital images.

3.2. SE(B) experiments

SE(B) test was selected in this research due to the simple geometry of the test specimens and simpler stress fields adjacent to the crack tip [47,48]. The supports were designed and developed in this research based on the ratios instructed in ASTM E1820-20b. The roller supports are designed with a diameter of 40 mm and a width of 100 mm. The net span length of the fixture is 320 mm, and the vertical load is applied on the top surface of the beam by a half roller with a diameter of 10 mm (w/8).

A crack mouth opening displacement (CMOD) gauge was mounted in the notch axis to capture crack openings while running each test. A minimum of 4-hour low-temperature conditioning time in the environmental chamber of the universal testing machine (UTM) was considered for the specimens prior to mounting the beams on the supports. The beams were placed on the fixture and the test was initialized by applying a preload of 0.1 kN to make the beam entirely seated on the supports. The experiments were carried out in CMOD control with a time to the

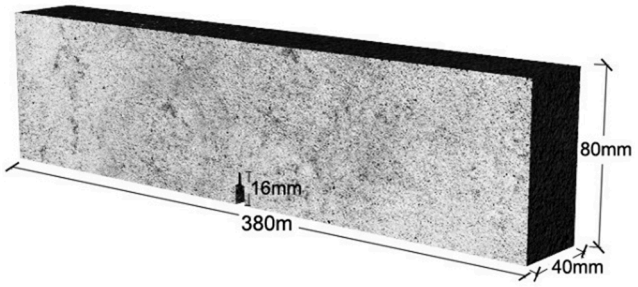

Fig. 3. AC beam dimensions and the fabricated mechanical notch in the centerline.

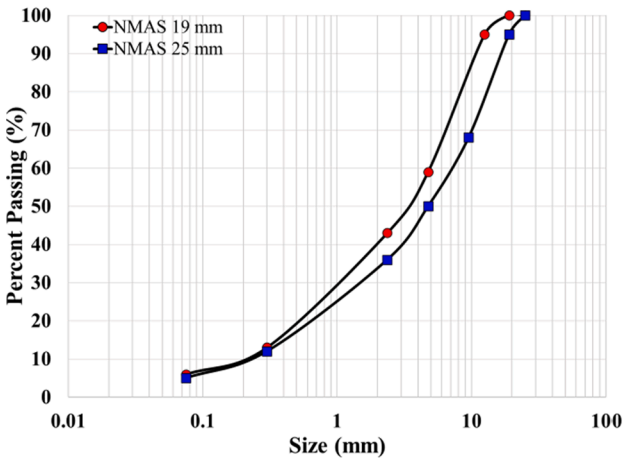

(a)

(b)

Fig. 2. Aggregate gradation (a), and crumb rubber powder (b).

peak load of 5 to 7 [48] seconds, and vertical load-line displacements and the CMOD increments were continuously logged during loading by the UTM data logger. Fig. 4(a) presents sample load-CMOD curves for the samples tested in 0 °C [49].

The test setup can be seen in Fig. 4(b). Two high-resolution digital cameras with resolutions of 18 and 20 Megapixels were installed facing the two sides of the beam to capture images at 5 and 15 frames per second continuously. LED bulb pads were also mounted on the side of each camera to provide the required illumination without inducing temperature disturbance inside the environmental chamber. Image capturing was triggered as the loading initiated for each test. The stored images were synchronized with the corresponding values of load, load-line displacement, and CMOD using a computer code. The open-source image analysis package (imageJ) was used to determine the crack length in each selected image.

3.3. Fracture parameters based on the R-curve method

Fracture resistance curves are constructed for each mixture in this research by plotting the cumulative fracture energy as a function of crack length. The cumulative fracture energy is computed based on the area under the load-LLD curves at every load step as the energy dissipated in creating the corresponding vertical deflection. R-curve is then generated by plotting the magnitude of the cumulative fracture energy versus the corresponding crack extension increment (Δa) at the considered load step. The crack extension is measured by analyzing the load-synchronized images. Therefore, in this fashion, the R-curve exhibits the energy dissipation trend in the mixtures at each test condition.

Moreover, the dissipated energy comprises multiple components such as the elastic strain energy, dissipated creep energy, dissipated fracture energy, etc. [11]. A sample R-curve is depicted in Fig. 5. By loading the beam specimen, R-curve rises vertically. This vertical state of the R-curve is attributed to the dissipation of cohesive energy for creating a plastic wake leading to the formation of cohesive crack surfaces. No or negligible crack extension can be seen in the captured images in this phase. As loading continues, the cohesive phase undergoes a transition to the propagation phase. Crack propagation can be stable or unstable, which can influence the size and extent of the transition zone [50]. The transition is proceeded by unstable crack propagation up to the failure of the specimen. The three R-curve-driven parameters proposed by Yang and Braham [18] are used in this research to quantify the R-curve: fracture energy (FE), cohesive energy (CE), and energy rate (ER). Based on the aforementioned method in constructing the R-curves,

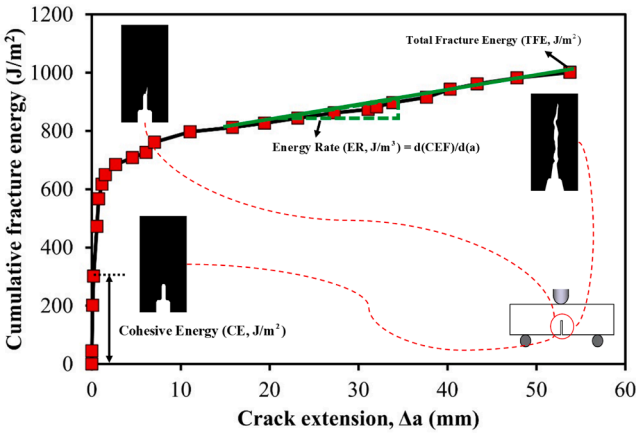

Fig. 5. Sample R-curve for crumb rubber modified mixtures tested at −20 °C and the quantitative fracture parameters.

the right-most point in each R-curve is identical to the fracture energy of the specimen, being the total energy dissipated in the fracture process of the AC beam. The cohesive energy corresponds to the coalescence of microvoids in the fracture process zone to form cracked surfaces. In this phase, energy is dissipated in a cohesive process to separate the two surfaces in the crack tip before initiating visible crack advance. Hence, the cohesive energy equals the vertical portion of each R-curve. The energy rate parameter is employed to present a measure of the energy required to advance the crack in the propagation zone. Hence, the energy rate definition can be written as in Eq. (1) [18]:

$$ER = \frac{FE - CE}{TCE} \tag{1}$$

Where:

ER: Energy rate, unit energy dissipated in crack propagation (J/m^3),

FE: Fracture energy, the total energy dissipated in both crack initiation and propagation (J/m^2), and.

TCE: Total crack extension, the crack length measured by image analysis on the beam surface (mm).

3.4. Environmental index

An environmental index is developed in this research comprising CO_2 and CH_4 emissions and the consumed energy to quantitatively

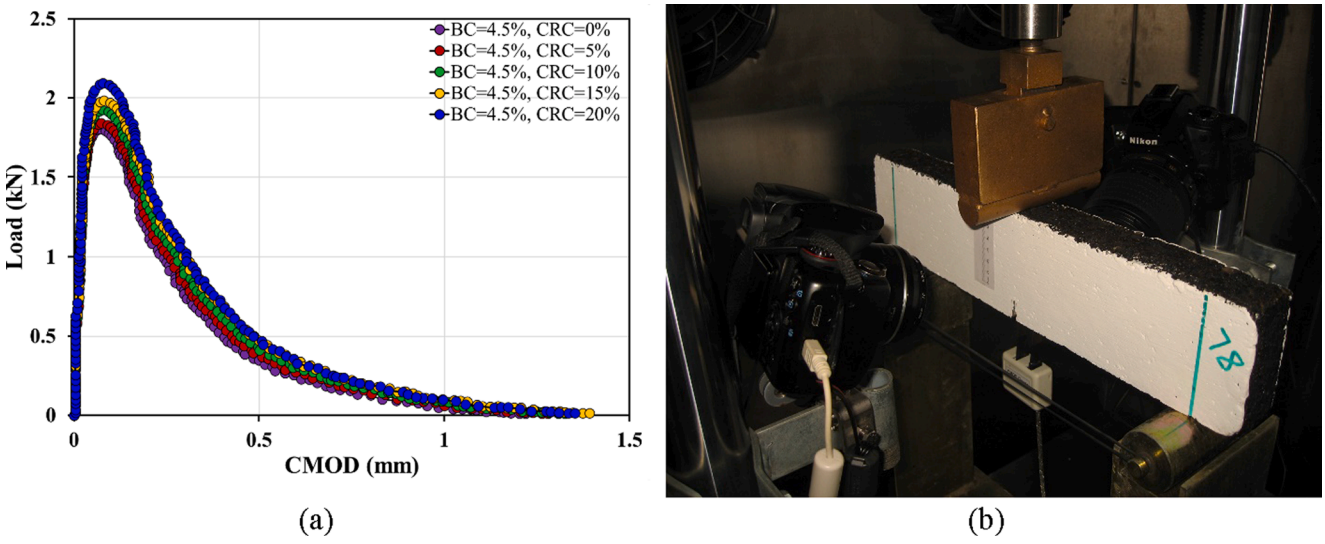

Fig. 4. Load versus CMOD for mixtures at T = 0 °C (a), and test setup (b).

assess the magnitude of pollution caused by the AC production. Thus, mixture proportions (aggregate and bitumen weights) were calculated for each laboratory sample (AC beams) and the CO_2, and CH_4 emissions, as well as the energy consumption for production of laboratory AC samples were assigned to each component according to the values in Table 3 to determine the pollution caused by production of each specimen [26,27,51,52].

The three factors: CO_2, CH_4 emissions, and energy consumption, should be combined to develop a unified environmental index. However, the factors mentioned are of incompatible ranges, i.e., the consumed energy ranges from 1.4 to 1.7 while the CH_4 emission falls between 0.002 and 0.01. Therefore, the value of each factor is scaled between 0 and 1 using Eq. (2)[53]:

$$N_i = \frac{i - i_{\min}}{i_{\max} - i_{\min}} \quad (2)$$

Where:
N_i: Normalized value of the environmental factor,
i: Actual value of the environmental factor,
i_{max}: Maximum value of the environmental factor, and,
i_{min}: Minimum value of the environmental factor.

Adding the three normalized factors, a cumulative environmental index is resulted, which ranges from 0 to 3 (Table 6). This index has a direct relationship with the environmental pollution caused by AC production. In other words, larger magnitudes of the cumulative environmental factor address higher environmental pollution by producing asphalt concrete.

3.5. Cost

Roadways are among the most important assets of each nation, and considerable budgets are allocated each year. Globally, above 400 billion US dollars are spent annually on pavement construction, maintenance, and rehabilitation [54]. Incorporating economic aspects of pavements could benefit the final designs by engineers. In the present research, the cost of producing laboratory specimens is calculated based on the local unit costs for each AC component as reported in Table 4. The cost of each component is scaled by Eq. (2) to a value between 0 and 1 (Table 6).

3.6. Design of experiments

An experimental design based on the central composite design (CCD) is applied to analyze the relationship between the considered factors and responses using RSM. CCD is an effective and prevalent method in RSM. In this method, the response surface curvatures are determined by the points located in the center of the experimental domain (center points) and axial points outside the experimental domain [55,56]. The primary advantage of this method is that the behavior of the experiments can be extracted with good precision requiring fewer experiments than a full-factorial design [40,55–57]. The main factors, their levels, and range of variation in the applied CCD are presented in Table 5.

As shown in Table 5, a face-centered CCD is employed to model and optimize the process using RSM. In this type of CCD, the axial points are located on the faces of the experimental domain, and each factor requires three levels [55–57]. The applied CCD is schematically presented in Fig. 6.

In this research, aggregate type (AT) and nominal maximum aggregate size (NMAS) are analyzed as two categoric factors with two levels. Moreover, binder content (BC), crumb rubber content (CRC) contents, and temperature (T) are considered as continuous factors with three levels consisting of lower, upper, and zero levels. The range of variation for BC, CRC, and T are 4 % to 5 %, 0 % to 20 %, and −20 °C to 0 °C, respectively. The Fracture responses being the mean value from three test replicates, cost, and environmental indices of the experiments based on the considered CCD are provided in Table 6.

Table 3
The energy consumption, CO_2, and CH_4 used in asphalt concrete.

Process	Energy consumption (MJ/Ton)	CO_2 emission (kg/Ton)	CH_4 (gr/Ton)
Siliceous aggregate production	54	10	0.0004
Limestone aggregate production	79.6	4.1	3.077
Binder production	5810	312	23
Crumb-rubber	62	21	7.13
HMA operation	275	22	0.005

Table 4
The unit price of asphalt concrete components.

Process	Unit price (USD ($)/Ton)
Siliceous aggregate production (NMAS = 19)	22.3
Siliceous aggregate production (NMAS = 25)	22.0
Limestone aggregate production (NMAS = 19)	25.8
Limestone aggregate production (NMAS = 25)	25.4
Binder production	1500
Crumb-rubber production	420
HMA operation	12

Table 5
Main factors and levels in CCD.

Factor	Code	Unit	Coded Level		
			−1	0	1
Binder Content (BC)	X_1	%	4	4.5	5
Crumb Rubber Content (CRC)	X_2	%	0	10	20
Temperature (T)	X_3	°C	−20	−10	0
Aggregate Type (AT)	X_4	–	Limestone (A)	–	Siliceous (B)
Nominal Maximum Aggregate Size (NMAS)	X_5	mm	19	–	25

4. Results and discussion

4.1. Experimental results (crack propagation analysis)

Fracture resistance curves are determined for all the mixtures within the scope of this research program. Sample R-curves at −20 °C are presented in Fig. 7(a) for mixtures with limestone aggregate and in Fig. 7 (b) for mixtures with siliceous aggregate. Unmodified and crumb rubber-modified AC mixtures are shown. The cohesive energy dissipation zone of the R-curve is proceeded by a transition zone to the unstable crack propagation phase. This zone includes the stable crack growth phase and has notable sizes for all the test conditions except at −20 °C. A 10 % crumb rubber modification has increased the height of the blunting fraction of the R-curves compared to the unmodified ones. The same trend can be seen for mixtures incorporating 20 % crumb rubber. The unmodified mixtures tend to undergo a brittle fracture at −20 °C, this can be noted by the flat R-curves for both aggregate types. As can be seen in Fig. 7(a) and Fig. 7(b), the R-curve proceeds substantially flat in the propagation region after 10 % crumb rubber modification as well. However, by incorporating 20 % crumb rubber, the unstable propagation fraction of the R-curves exhibits a distinct rising inclination. This progressively rising R-curve in 20 % crumb rubber modified samples is a desirable material property attributed to the reinforcing effect of crumb rubber particles causing improved energy dissipation as the crack extends in the instability region. In other words, 20 % crumb rubber-modified mixtures are exhibiting a higher resistance against low-temperature unstable crack propagation.

The effect of binder content and gradation of the mixtures are

Table 6
Results of CCD-based experimental design.

Run No.	Factors					Fracture Response			Cost	Env
	BC (%)	CRC (%)	T (°C)	AT	NMAS	CE	FE	ER		
1	4	0	−20	A	19	300	572	1.4124	0.2522	1.4765
2	4	0	−20	A	25	289	599	1.257	0.1261	1.1245
3	4	0	−20	B	19	186	457	0.4911	0.1190	0.8786
4	4	0	−20	B	25	223	417	0.2043	0.0000	0.5460
5	4	0	0	A	19	74	380	1.3519	0.2522	1.4765
6	4	0	0	A	25	138	399	1.8739	0.1261	1.1245
7	4	0	0	B	19	96	280	1.882	0.1190	0.8786
8	4	0	0	B	25	99	278	1.577	0.0000	0.5460
9	4	10	−10	A	19	98	809	4.0574	0.3153	1.4876
10	4	10	−10	A	25	110	930	2.0813	0.1873	1.1352
11	4	10	−10	B	19	131	709	2.4811	0.1827	0.8922
12	4	10	−10	B	25	150	817	4.9966	0.0617	0.5591
13	4	20	−20	A	19	366	583	3.1212	0.3784	1.4986
14	4	20	−20	A	25	418	588	2.771	0.2484	1.1459
15	4	20	−20	B	19	228	482	1.555	0.2464	0.9057
16	4	20	−20	B	25	267	492	1.0811	0.1233	0.5722
17	4	20	0	A	19	101	458	2.999	0.3784	1.4986
18	4	20	0	A	25	114	480	3.0062	0.2484	1.1459
19	4	20	0	B	19	101	308	1.9933	0.2464	0.9057
20	4	20	0	B	25	118	310	1.9838	0.1233	0.5722
21	4.5	0	−10	A	19	100	695	1.7139	0.5472	1.9473
22	4.5	0	−10	A	25	118	741	1.257	0.4117	1.5800
23	4.5	0	−10	B	19	110	586	1.66	0.4148	1.3526
24	4.5	0	−10	B	25	252	605	1.3854	0.2862	1.0045
25	4.5	10	−20	A	19	305	641	2.7111	0.6182	1.9597
26	4.5	10	−20	A	25	358	672	2.4421	0.4805	1.5921
27	4.5	10	−20	B	19	262	588	0.639	0.4864	1.3678
28	4.5	10	−20	B	25	312	604	0.1001	0.3556	1.0193
29	4.5	10	−10	A	19	101	846	4.444	0.6182	1.9597
30	4.5	10	−10	A	25	114	857	4.5241	0.4805	1.5921
31	4.5	10	−10	B	19	202	722	5.228	0.4864	1.3678
32	4.5	10	−10	B	25	224	731	5.1976	0.3556	1.0193
33	4.5	10	0	A	19	86	486	2.639	0.6182	1.9597
34	4.5	10	0	A	25	97	500	2.6755	0.4805	1.5921
35	4.5	10	0	B	19	122	371	2.492	0.4864	1.3678
36	4.5	10	0	B	25	145	374	2.5379	0.3556	1.0193
37	4.5	20	−10	A	19	166	899	4.269	0.6892	1.9722
38	4.5	20	−10	A	25	197	933	4.2726	0.5492	1.6041
39	4.5	20	−10	B	19	183	801	5.191	0.5580	1.3831
40	4.5	20	−10	B	25	211	802	5.2614	0.4249	1.0340
41	5	0	−20	A	19	492	812	1.893	0.8422	2.4181
42	5	0	−20	A	25	468	903	1.3801	0.6972	2.0356
43	5	0	−20	B	19	312	723	0.6047	0.7105	1.8265
44	5	0	−20	B	25	301	732	0.3144	0.5724	1.4631
45	5	0	0	A	19	96	599	6.1405	0.8422	2.4181
46	5	0	0	A	25	285	696	3.6596	0.6972	2.0356
47	5	0	0	B	19	190	532	4.3049	0.7105	1.8265
48	5	0	0	B	25	218	561	3.124	0.5724	1.4631
49	5	10	−10	A	19	145	822	6.281	0.9211	2.4319
50	5	10	−10	A	25	168	942	3.2981	0.7736	2.0490
51	5	10	−10	B	19	248	728	6.3944	0.7901	1.8434
52	5	10	−10	B	25	295	758	6.4815	0.6495	1.4795
53	5	20	−20	A	19	531	974	1.247	1.0000	2.4458
54	5	20	−20	A	25	582	996	4.228	0.8501	2.0623
55	5	20	−20	B	19	348	771	1.4421	0.8696	1.8604
56	5	20	−20	B	25	397	805	1.4444	0.7266	1.4959
57	5	20	0	A	19	147	701	6.4831	1.0000	2.4458
58	5	20	0	A	25	375	745	6.4534	0.8501	2.0623
59	5	20	0	B	19	251	571	4.6719	0.8696	1.8604
60	5	20	0	B	25	298	592	4.7258	0.7266	1.4959

depicted at the highest and lowest test temperatures in Fig. 8(a) and Fig. 8(b), respectively. It can be observed that using a larger maximum aggregate size has not changed the overall fracture regime of the mixtures; however, a slight rise in the R-curves can be noted. This overall rise in the R-curve leads to increasing the cohesive energy and fracture energy of the mixtures while the energy rate may not necessarily change. Furthermore, and for each gradation, increasing the binder content has led to a notable rise in the R-curves. Increasing the amount of binder at each mixture provides further coating of the aggregate and a stronger bond between the aggregate and the bitumen, leading to higher energy dissipations for initiating and advancing the crack tip. Comparing Fig. 8 (a) and Fig. 8(b) also indicates that despite the cohesive/blunting fraction of the R-curve is risen by reducing the temperature, the tendency for initiation of unstable crack growth is increased which can be inferred by the notably smaller stable crack growth region of the R-curves in Fig. 8 (b).

4.2. Statistical analysis

In this research, the crack propagation properties of asphalt concrete

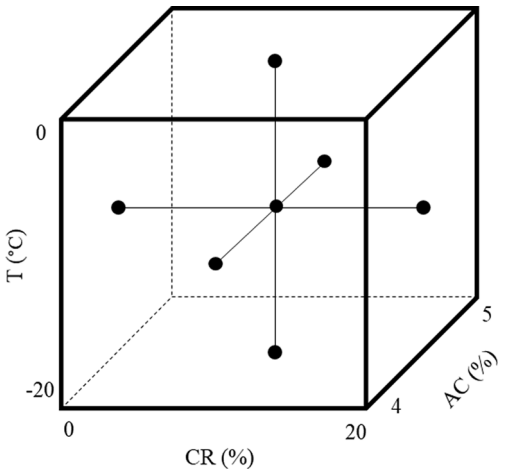

Fig. 6. Applied face-centered CCD.

mixtures (cohesive energy, fracture energy, and energy rate) are evaluated considering five main factors: aggregate type, nominal maximum aggregate size, binder content, crumb rubber content, and temperature; with design of experiments based on the faced-centered CCD (Table 5). The statistical analysis of the experimental data is presented and elaborated in the following sections.

4.2.1. Model generation

As the first step in RSM, the influence and interactions of the main factors on the experimental responses are statistically analyzed using analysis of variance (ANOVA) by Design Expert 12 software. The significance level of the factor effect can be evaluated by its p-value. In general, factors with p-values>0.1 are considered insignificant factors, and those with 0.1 < p-value < 0.05 have minor significance. Whereas factors with p-value<0.05 significantly influence the response and have high significance level [58,59] In this research, the models were developed using highly significant factors (p-value < 0.05).

For modeling the behavior of the experimental responses versus the variations in the considered factors, multiple types of model structures such as linear, quadratic (second-order), and cubic (third-order) were evaluated, and the ANOVA is used to determine the significance of each term in the structure of the model for simulating the experiment responses. Finally, after eliminating the insignificant terms (p-value > 0.05), a simplified polynomial model was generated for each response. The coded equations of the generated models and their statistical efficiency are presented in Eq 3–5.

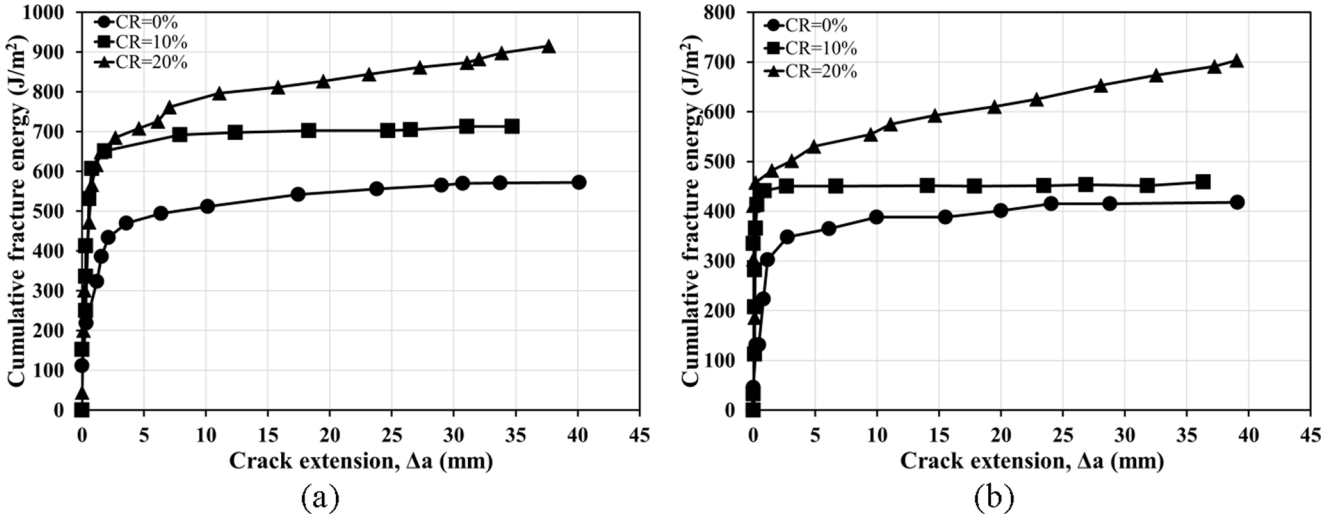

Fig. 7. R-curves for unmodified and crumb rubber modified mixtures with (a) limestone aggregate, and (b) siliceous aggregate.

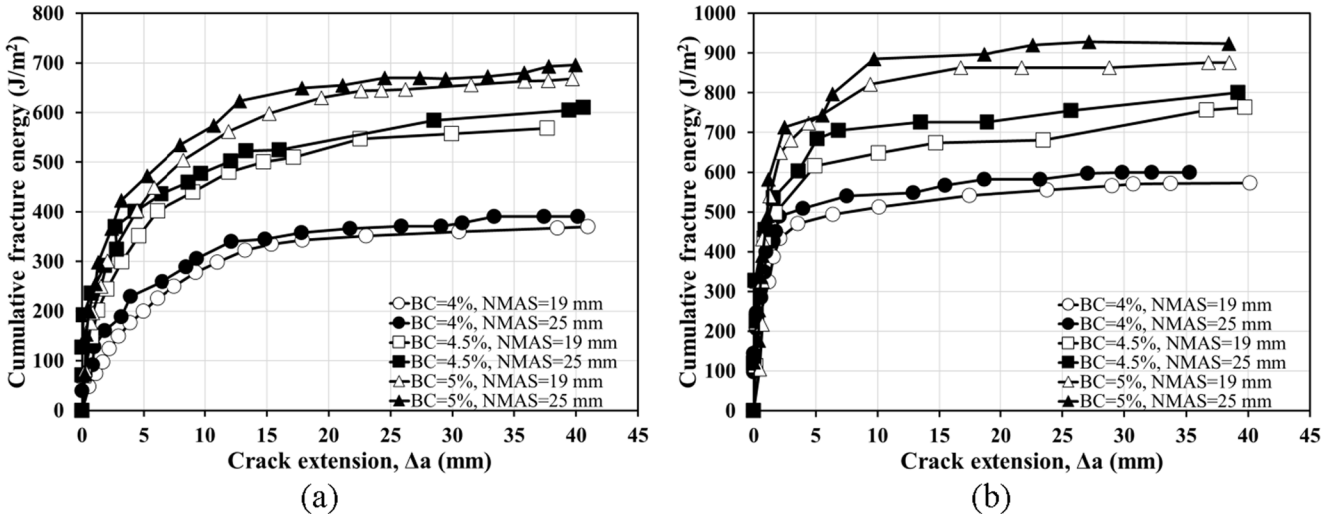

Fig. 8. Effect of binder content and NMAS at two temperature levels of (a) 0 °C, and (b) −20 °C.

$$\begin{cases} CE = 147.04 + 63.50X_1 + 26.30X_2 - 94.85X_3 + 34.45X_4 + 21.05X_5 + 34.95X_3X_4 + 24.39X_1X_1 + 23.39X_2X_2 \\ +67.14X_3X_3 + 13.97X_1X_3X_5 - 63.15X_3X_3X_4 \\ R^2 = 0.9195\ ,\ R^2_{adj} = 0.9010\ ,\ R^2_{pred} = 0.8735\ ,\ Adequate\,precision\ = 27.1587 \end{cases} \tag{3}$$

$$\begin{cases} FE = 765.50 + 115.37X_1 + 101X_2 - 94.75X_3 - 62.52X_4 + 15.88X_5 + 52.88X_1X_1\ - 232X_3X_3 - 72.38X_1X_1X_2 \\ R^2 = 0.9098\ ,\ R^2_{adj} = 0.8957\ ,\ R^2_{pred} = 0.8777\ ,\ Adequate\,precision = 31.7887 \end{cases} \tag{4}$$

$$\begin{cases} ER = 3.94 + 0.8099X_1 + 1.62X_2 + 0.9059X_3 + 0.4039X_4 + 0.6949X_1X_3 + 0.7953X_1X_1\ - 0.5874X_2X_2 - 1.68X_3X_3 \\ -1.07X_1X_1X_2 - 0.9683X_3X_3X_4 \\ R^2 = 0.8386\ ,\ R^2_{adj} = 0.8056\ ,\ R^2_{pred} = 0.7619\ ,\ Adequate\,precision = 16.5171 \end{cases} \tag{5}$$

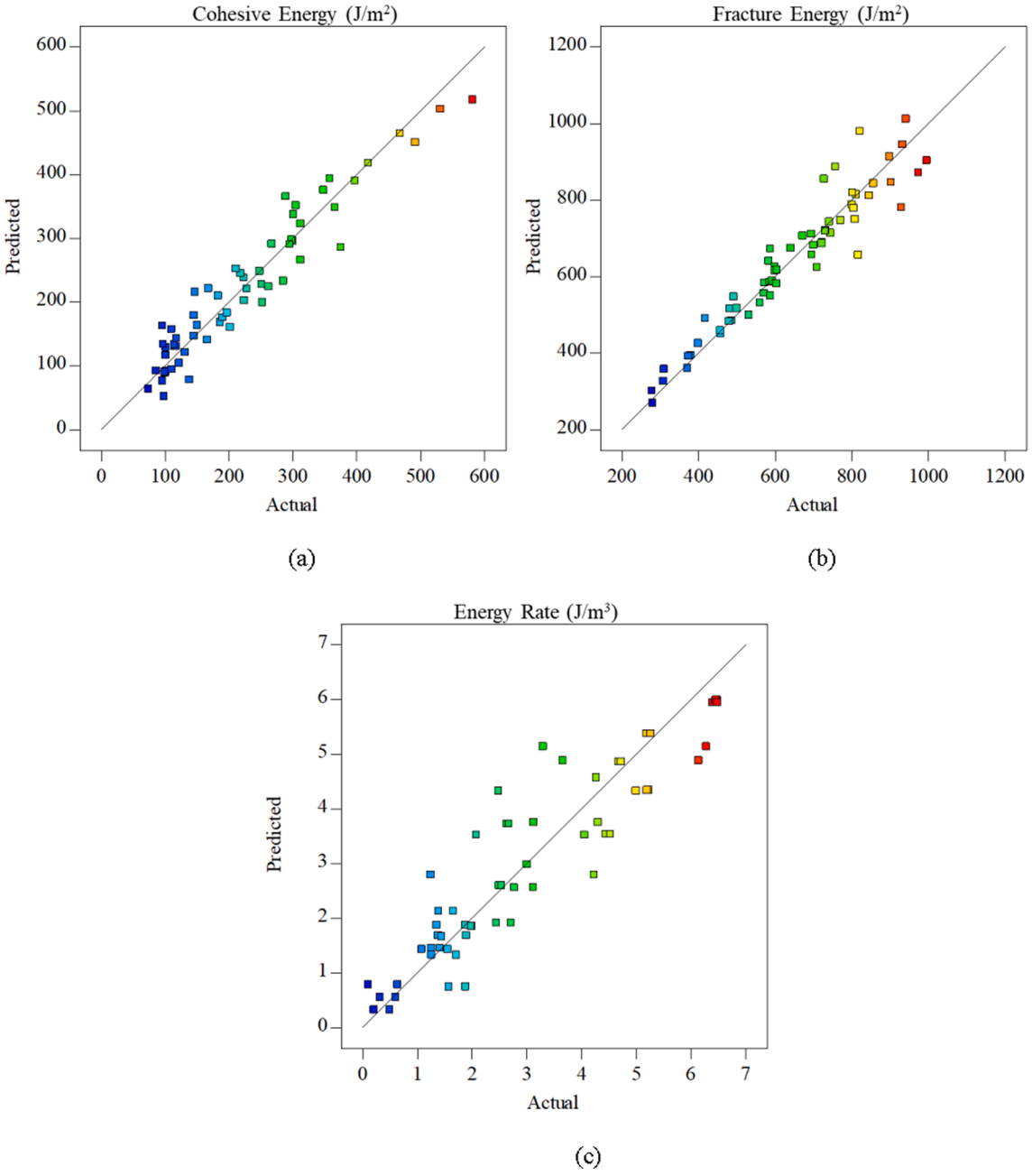

Fig. 9. Performance of the generated models.

According to Eq 3–5, the R^2 values indicate that the models provide an acceptable representation of experimental trends with values of 0.9195, 0.9098, and 0.8386 for CE, FE, and ER, respectively. Also, as shown in Fig. 9, a favorable similarity between model predictions and real experimental responses can be seen.

Moreover, the values of Adjusted-R^2 (R^2_{adj}) are close to R^2, which indicates that the generated models are not over-parametrized, with a suitable structure. Also, the difference between R^2_{adj} and R^2_{pred} is<0.2 in all models, which indicates that the models have an acceptable performance. The statistical parameter, Adequate precision, was considered to evaluate the signal-to-noise ratio in the responses of the models. The desirable value for this index is greater than four [57]. Hence, the generated models have adequate signals with 27.1587, 31.7887, and 16.5171 for CE, FE, and ER, respectively. Finally, the comparison of the predicted versus the actual values in Fig. 9 shows that the models are acceptable in predicting the experimental responses.

p-values are presented in Table 7, which indicates the influence of each factor on the models. In addition, the correlation between factors and responses can be compared according to the coefficient of the engaged factors in the models.

As shown in Table 7, the main factors considered (AT, NMAS, BC, CRC, and T) have an extremely significant effect on cohesive energy with a p-value < 0.0001. Based on the coefficient of factors, the temperature and BC have the greatest correlation with CE in negative and positive directions, respectively. Also, it can be inferred that the main factors have a significant effect on the variations of the fracture energy, but the effect of the NMAS is less than other main factors. The positive correlation of BC and CRC with FE is higher than other factors and their interactions. On the other hand, the temperature has the greatest negative correlation with fracture energy.

Analysis of the factors in the generated model for energy rate (presented in Table 7) indicates that NMAS and its interactions with other factors have no significant effect on this fracture parameter. Also, aggregate type has the least effect on ER than the other main factors (BC, CRC, and T), which have an extremely significant influence on cohesive energy according to p-value < 0.0001. The CRC factor has the highest positive correlation with cohesive energy based on the coefficient values.

According to the results of ANOVA (Table 7), the p-values of the generated models indicate a fundamental relationship between the model predictions and experimental responses with a p-value < 0.0001.

In the next step, contour plots were outlined to provide more information on the relationship between the investigated factors and responses. The interaction among the effective factors (p-value < 0.05) on CE, FE, and ER are presented in Figs. 10-12, respectively.

Regarding Fig. 10, increasing the binder content in all the mixtures has raised the cohesive energy regardless of the aggregate type and crumb rubber modification. This effect could previously be interpreted from the R-curves for temperature levels of 0 °C and −20 °C and binder contents of 4 %, 4.5 %, and 5.0 % in Fig. 8(a) and 8(b), nevertheless, a continuum space of cohesive energy magnitudes with continuous variations of binder content and temperature is obtained through RSM in Fig. 10.

Comparing Fig. 10(a) and 10(b), it can be seen that incorporation of crumb rubber up to 20 % has led to increasing the cohesive energy. In Fig. 10(b), the cohesive energy falls within a range of 100 J/m^2 up to −11 °C even at binder contents above the optimal value (4.5 %). In contrast, in 20 % crumb rubber modified mixtures, a larger domain of temperatures can be seen at binder contents lower than 4.5 % surrounded by the 200 J/m^2 contour. This is indicating the highly positive effect of crumb rubber particles in reinforcing the AC matrix causing higher energy dissipations for forming cohesive surfaces before crack initiation. Comparing Fig. 10(b) with 10(c) shows that the cohesive energy is slightly lower at higher temperatures for mixtures with siliceous aggregate.

However, as the temperature is reduced, the cohesive energy drops significantly at the same binder content for siliceous aggregate. This effect can be addressed regarding the poor adhesion of the siliceous aggregate with bitumen [60]. Given the weaker bond ability of the siliceous aggregate in addition to the relatively lower coating of this aggregate type in comparison with limestone (Table 1), a higher tendency of crack initiation in these mixtures can be seen resulting in lower magnitudes of cohesive energy. Fig. 10(d) shows that incorporating 20 % crumb rubber has significantly contributed to improving the undesirably lower cohesive energy resulting from higher binder absorption of the siliceous aggregate. However, considering Fig. 10(a), crumb rubber incorporation has had a more pronounced effect in increasing the cohesive energy for mixtures with limestone. This phenomenon can be further confirmed by comparing Fig. 10(f) and Fig. 10(h), where 20 % crumb rubber modification is considered for mixtures with the two types of aggregates having a maximum nominal size of 19 mm. While the modified limestone mixtures are approaching a cohesive energy of 500 J/m^2 at 5 % binder content, the cohesive energy by addition of crumb rubber to the siliceous mixtures has remained below 400 J/m^2, which is indicating that the higher absorption of the siliceous aggregate imposes a significant loss of bond between the aggregate and the binder and impairs the reinforcing effect of crumb rubber particles compared to the limestone mixtures.

Considering the unmodified mixtures, increasing the binder content does not cause significant changes in the fracture energy at each temperature level. However, a slightly more pronounced increase in the fracture energy can be observed as the binder content is increased beyond 4.6 % (beyond the optimum content). For both NMAS values and both aggregate types, a more consistent increase in fracture energy can be observed as the mixtures are crumb rubber modified which can be

Table 7
The results of ANOVA.

CE			FE			ER		
Source	p-value	Coef.	Source	p-value	Coef.	Source	p-value	Coef.
X_1	< 0.0001	63.50	X_1	< 0.0001	115.37	X_1	< 0.0001	0.81
X_2	< 0.0001	26.30	X_2	< 0.0001	101.00	X_2	< 0.0001	1.62
X_3	< 0.0001	−94.85	X_3	< 0.0001	−94.75	X_3	< 0.0001	0.91
X_4	= 0.0002	34.45	X_4	< 0.0001	−62.52	X_4	= 0.0287	0.40
X_5	< 0.0001	21.05	X_5	= 0.0467	15.88	X_1X_3	< 0.0001	0.69
X_3X_4	< 0.0001	34.95	X_1X_1	= 0.0050	52.88	X_1X_1	= 0.0025	0.79
X_1X_1	= 0.0465	24.39	X_3X_3	< 0.0001	–232.00	X_2X_2	= 0.0228	−0.59
X_2X_2	= 0.0559	23.39	$X_1X_1X_2$	= 0.0038	−72.38	X_3X_3	< 0.0001	−1.68
X_3X_3	< 0.0001	67.14				$X_1X_1X_2$	= 0.0015	−1.07
$X_1X_3X_5$	= 0.0444	13.97				$X_3X_3X_4$	< 0.0001	−0.97
$X_3X_3X_4$	< 0.0001	−63.15						
Model p-value < 0.0001						Model p-value < 0.0001		
			Model p-value < 0.0001					

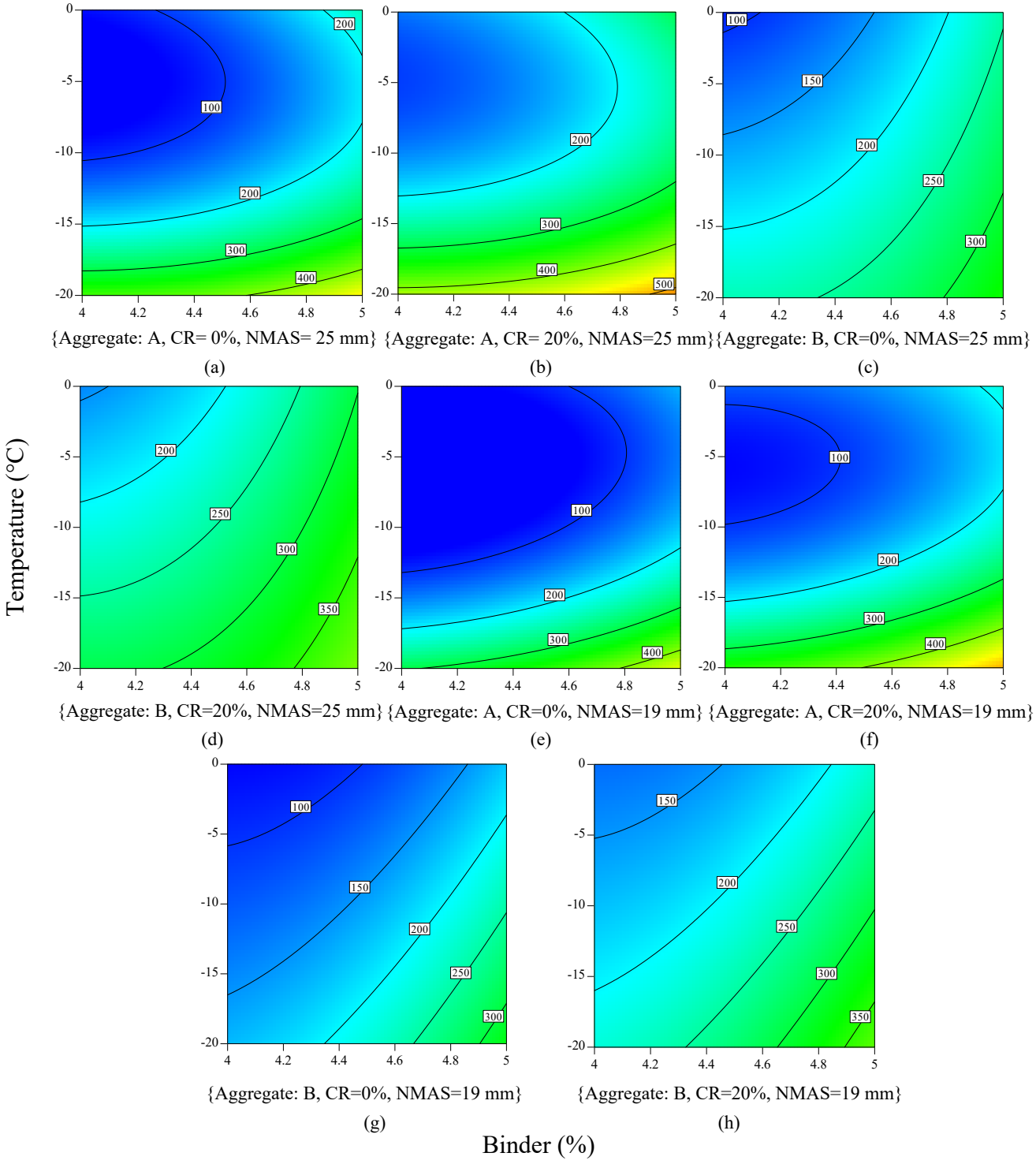

Fig. 10. CE trend of mixtures at various levels of the effective factors.

seen in Fig. 11(b), 11(d), 11(f), and 11(h). Saddle points can be noted in unmodified samples as in Fig. 11(a), 11(c), 11(e), and 11(g). Looking at Fig. 11(e), it can be observed for the mixtures with limestone and NMAS 19 mm, that regardless of the binder content of the mixtures, the fracture energy is increased as the temperature is reduced from 0 °C to approximately −12 °C due to the induced toughening in the mixture by the increased stiffness of the binder and strengthened bonding in the interface of the aggregate and the binder. However, the fracture energy drops as the temperature is reduced to below −15 °C and thereafter. This is emphasizing the presence of creep dissipations in higher temperature ranges than the lower ones here. At higher temperatures (above −15 °C in this research), the viscous process is present both before crack initiation and the propagation phase. While as the temperature is reduced to below −15 °C, a dominating elastic behavior leading to brittle fracture can be seen, resulting in lower fracture energy magnitudes at −20 °C than at higher temperatures. For each aggregate size, the magnitudes of fracture energy are higher for mixtures developed by limestone aggregate, which can be associated with substantial bond strength than the highly bitumen absorbing siliceous ones, as shown in Fig. 11(b) and 11 (e). For each aggregate type and size, incorporation of 20 % crumb

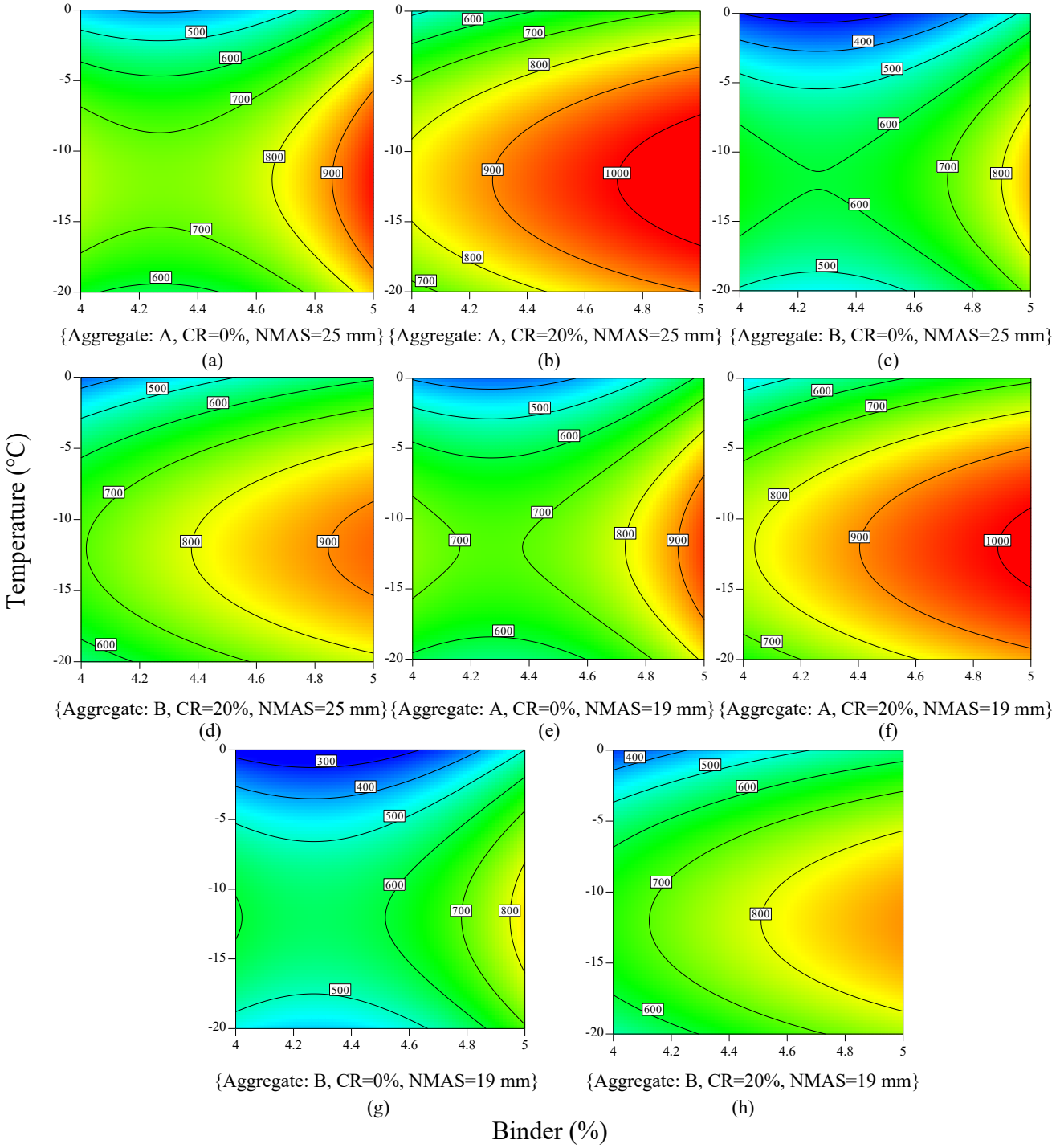

Fig. 11. FE trend of mixtures at various levels of the effective factors.

rubber has removed the saddle points in the contour plots as can be noted in Fig. 11(b), 11(d), 11(f), and 11(h). No significant chemical reaction occurs at moderate to low velocities of mixing the crumb rubber powder with the base binder, particularly at temperatures below 180 °C [61,62]. Therefore, the unreacted particles of crumb rubber swell and remain mechanically effective in reinforcing the binder and the matrix in the mixture without significant sensitivity to temperature variations which can be addressed as induced toughness from a fracture mechanics view. As a result, even at the lowest temperature levels in this research, where unmodified mixtures undergo brittle fracture, the higher toughness of the rubberized mixtures causes higher fracture energy magnitudes.

R-curves provide the means to characterize the post-peak fracture behavior of the materials. In this regard, energy rates for unmodified and modified mixtures with the two types of aggregate and NMAS 25 mm are presented in Fig. 12(a) to 12(d) to assess the crack propagation properties of each mixture. For unmodified mixtures, as can be seen in Fig. 12(a) and 12(c), increasing the binder content increases the energy rate at temperatures above −15 °C for limestone mixtures while increasing the binder is not very effective on mixtures with siliceous aggregate due to the lower bond strengths in such aggregate. The formation of saddle points in these two mixtures indicates that the energy

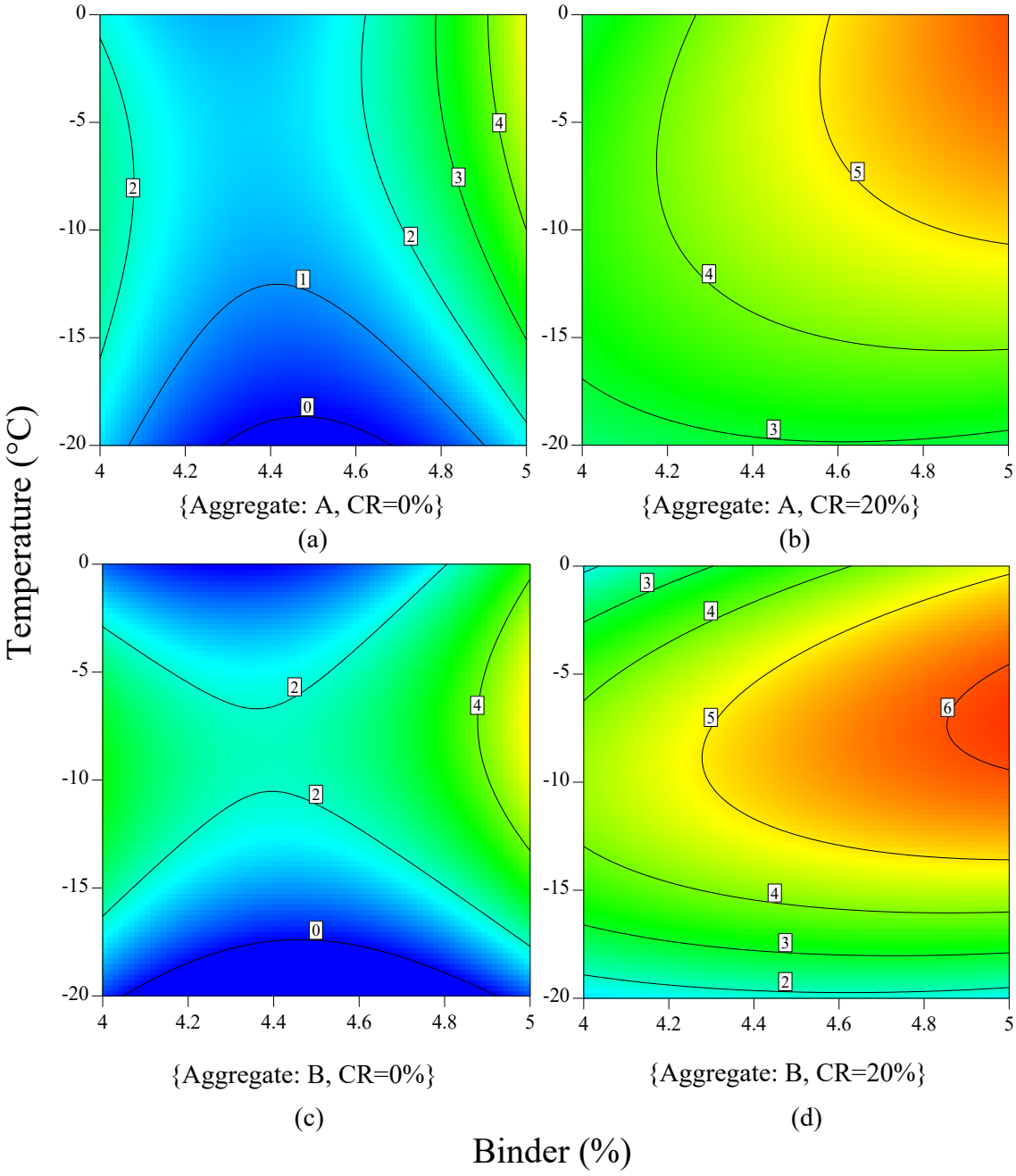

Fig. 12. ER regime of mixtures at various levels of the effective factors.

rate and the crack propagation intensity are not affected by changes of binder content at low temperatures, in both the unmodified mixtures, as the temperature is reduced to −15 °C and below, energy rates are seen to approach zero. A zero-energy rate corresponds to an entirely horizontal R-curve after the initiation of the macrocrack in the mixture, which addresses a totally unstable crack growth. This phenomenon occurs as the crack driving force dramatically exceeds the mixture's resistance, leading to an abrupt failure of the test sample or the AC layer in pavement structure, which is an undesirable effect. As the mixtures are crumb rubber modified, depicted in Fig. 12(b) and 12(d), the saddle point disappears, and increasing the binder content contributes to increasing the energy rate at each temperature. Zero energy rate is not observed in the modified mixtures, indicating the positive effect of crumb rubber incorporation at low temperatures in reducing the unstable crack growth in AC mixtures. In other words, and as can be seen from Fig. 7(a) and 7(b), the incorporation of 20 % crumb rubber has created a progressively rising R-curve of the mixtures even at the lowest temperature (-20 °C). This indicates that the reinforcing effect of crumb rubber particles in the mixtures has resulted in a notable resistance against crack propagation in the post-peak region within the instability phase of the R-curve.

4.2.2. *Model verification*

Several more experiments were carried out in this stage to validate the performance of the prediction models on new samples. These samples were created with the same material and following the same process as the RSM samples, however, the values of T and CRC differed from the levels considered in CCD.

The relative error (RE) was applied to evaluate the performance of the models in predicting fracture regime of the new samples (CE, FE, and

Table 8
Results of model verification process.

Run No.	Factors						Fracture Response		
	AT	BC (%)	CRC (%)	NMAS	T (°C)		CE	FE	ER
1	A	4	15	25	0	Experiment	111.1121	438.4444	3.2899
						Model	100.0451	468.9625	3.1476
						RE (%)	9.9594	6.9605	4.3246
2	A	4.5	5	25	−10	Experiment	123.0000	788.0000	2.8810
						Model	126.3361	793.4000	2.5787
						RE (%)	2.7123	0.6853	10.4919
3	B	4.5	5	19	−10	Experiment	136.7120	666.0000	3.4658
						Model	153.1361	636.6000	3.3866
						RE (%)	12.0137	4.4144	2.2853
4	B	5	0	19	−5	Experiment	210.0000	656.0000	5.1250
						Model	209.4795	721.3500	4.9453
						RE (%)	0.2479	9.9619	3.5054
5	B	4	20	19	−15	Experiment	200.8304	691.3330	3.2811
						Model	194.9795	642.6000	3.5282
						RE (%)	2.9133	7.0491	7.5299
6	B	4	15	25	0	Experiment	104.3384	369.8819	1.8003
						Model	112.5451	343.9292	2.0188
						RE (%)	7.8655	7.0165	12.1377
7	A	4	15	19	0	Experiment	79.0050	418.0000	3.6110
						Model	85.8826	437.1958	3.1476
						RE (%)	8.7053	4.5923	12.8321
						Mean RE (%)	6.3453	5.8114	7.5867

ER). The deviation of predicted values from experimental values are calculated using RE as follow:

$$RE(\%) = \left|\frac{Experiment - Prediction}{Experiment}\right| \times 100 \tag{6}$$

The value of factors in new samples and the performance of generated models based on the RE index are presented in Table 8.

As can be seen in Table 8, the generated models have a proper performance in predicting fracture properties of new samples. Additionally, performance of the models can be verified with mean RE values of 6.3453, 5.8114, and 7.5867 percent on CE, FE, and ER, respectively.

4.3. Multi-objective optimization of mix design

The fracture properties of AC mixtures can be predicted as the RSM-based models for extracting the behavior of the experimental responses are generated. Model verification results indicate that the RSM-based models can benefit in predicting fracture parameters with varying mixture properties such as the AT, NMAS, BC, and CRC, and test conditions, i.e., temperature level. Accordingly, the mix design parameters can be assessed based on various objectives. An optimization problem consists of objective functions, decision variables and constraints [63,64]. Equations 7–13 state the objective functions and constraints of the optimization problem:

$$\text{Maximum } F_1 = 147.04 + 63.50X_1 + 26.30X_2 - 94.85X_3 + 34.45X_4 + 21.05X_5 + 34.95X_3X_4 + 24.39X_1X_1 + 23.39X_2X_2 + 67.14X_3X_3 + 13.97X_1X_3X_5 - 63.15X_3X_3X_4 \tag{7}$$

$$\text{Maximum } F_2 = 765.50 + 115.37X_1 + 101X_2 - 94.75X_3 - 62.52X_4 + 15.88X_5 + 52.88X_1X_1 - 232X_3X_3 - 72.38X_1X_1X_2 \tag{8}$$

$$\text{Maximum } F_3 = 3.94 + 0.8099X_1 + 1.62X_2 + 0.9059X_3 + 0.4039X_4 + 0.6949X_1X_3 + 0.7953X_1X_1 - 0.5874X_2X_2 - 1.68X_3X_3 - 1.07X_1X_1X_2 - 0.9683X_3X_3X_4 \tag{9}$$

$$\text{Minimum } F_4 = 0.4852 + 0.2984 \times X_1 + 0.0702 \times X_2 - 0.0642 \times X_4 - 0.0671 \times X_5 \tag{10}$$

$$\text{Minimum } F_5 = 1.48 + 0.4662 \times X_1 + 0.0136 \times X_2 - 0.2912 \times X_4 - 0.1790 \times X_5 \tag{11}$$

$$X_i \le Maximum(X_i) \quad \forall i \in \{1,2,3,4,5\} \tag{12}$$

$$X_i \ge \text{Minimum}(X_i) \quad \forall i \in \{1,2,3,4,5\} \tag{13}$$

S.t.

where X_1, X_2, X_3, X_4, and X_5 are the binder content, crumb rubber content, temperature, aggregate type, and nominal maximum aggregate size. F_1, F_2, and F_3 are the objective functions of CE, FE, and ER, respectively. Cost and ENV objective functions are also shown with F_4 and F_5, which should be minimized.

In this research, various optimization scenarios are examined to reach the optimal mix design with maximum fracture responses, minimal mixture costs and environmental concerns. Multi-objective optimization results are summarized in Table 9.

Two sets of optimization scenarios are applied to reveal the possible effects of incorporating environmental and budget concerns in mixture design. A stand-alone multi-objective optimization is utilized for maximizing the fracture responses of the asphalt mixture (CE, FE, and ER) in low temperature conditions, while a multi-objective optimization for maximizing the fracture responses simultaneously with minimizing the

Table 9
Multi-objective optimization.

Optimization scenarios		Temperature (°C)	Mixture parameter				Optimum responses				
Maximize	Minimize		BC (%)	CRC (%)	NMAS (mm)	AT	CE	FE	ER	Cost	ENV
CE, FE and ER	–	0	5	20	25	A	285.674	714.025	5.990	0.851	2.078
CE, FE and ER	Env and cost		4.77	20	25	B	247.760	551.980	4.395	0.588	1.285
CE, FE and ER	Env and cost		5	0	25	B	245.570	531.742	3.756	0.582	1.466
CE, FE and ER	–	−10	5	20	25	B	340.120	915.740	5.920	0.720	1.490
CE, FE and ER	Env and cost		4.74	19.5	25	B	288.710	871.180	5.710	0.570	1.250
CE, FE and ER	Env and cost		5	0	25	B	287.500	858.500	4.810	0.580	1.470
CE, FE and ER	–	−20	5	20	25	B	340.117	915.742	5.917	0.722	1.496
CE, FE and ER	Env and cost		4.74	20	25	B	288.699	871.167	5.708	0.569	1.255
CE, FE and ER	Env and cost		5	0	25	B	287.517	858.492	4.808	0.582	1.466

cost and environmental factors associated with the mixtures is carried out as well. The last row for each temperature in Table 9 presents the optimum mix design (according to low temperature fracture responses of the asphalt mixture) for the reference mixture with CRC = 0 which can be compared to the crumb rubber modified mixture incorporating fracture performance, costs, and environmental indices simultaneously.

As can be seen in Table 9, the optimization results reveal that the optimum mix design for maximizing the fracture responses of the asphalt mixtures in −10 °C comes with 5 % binder content while the crumb rubber is found to be 20 %. Moreover, a maximum aggregate size of 25 mm has led to optimum responses in all optimization scenarios.

Applying the second scenario in which mixture fracture responses are maximized simultaneously with a minimization of costs and environmental concerns, a value of 4.74 % is resulted as the optimum binder content at −10 °C and −20 °C. It should be noted that, in maximizing the fracture behavior while minimizing the environmental effects, the CRC constantly equals 20 % which agrees with the findings of Wang [33] about the environmental benefits of crumb rubber addition to asphalt concrete mixtures.

At the temperature of −10 °C, the maximum magnitudes of cohesive energy, fracture energy, and energy rate correspond to the first scenario where costs and environmental target functions are not considered. However, as the costs and environmental functions are also minimized in the second scenario, the fracture indices diminish negligibly while the costs and environmental effects are significantly reduced. The environmental index comprising CO_2 and CH_4 is reduced up to 16.1 %, and the reduction for costs is approximately 21 %. In 0 °C and −20 °C, the reduction of environmental effects is approximately 38 % and 16 %, and the cost reduction is almost 31 % and 21 %, respectively.

Comparing the results of the second scenario in crumb rubber modified and the reference mix design (CRC = 0), it can be seen that the environmental factor was reduced by 15 %, a conservation of 1.7 % in costs was achieved, and more desirable fracture responses have been resulted in −10 °C. In addition, at temperatures of 0 °C and −20 °C, the environmental factor is reduced by 12 % and 14 %, respectively. The cost of the mixture remains the same at 0 °C, and it has been decreased by 2.3 % at −20 °C compared to the reference mix design.

5. Conclusions and future work

Unmodified and crumb rubber modified AC mixtures with limestone and siliceous aggregate with three binder contents were tested under SE (B) fracture testing protocol to obtain fracture resistance curves of the mixtures at three temperature levels ranging from 0 °C to –20 °C. Three parameters were extracted from each R-curve to quantify the crack propagation trend of each mixture. RSM was applied to develop the best model between the fracture performance, costs, environmental factor, as well as the mixture properties, and the results were optimized using multi-objective scenarios. The following conclusions can be summarized:

- R-curves provide a robust tool for characterizing the entire fracture and crack propagation trend of AC mixtures. However, derivation of these curves entails significant experimental costs and difficulties. The RSM could serve as an efficient approach in extracting the behavior of the R-curve-driven parameters and hence the optimization of the AC mixtures.
- In the RSM process, factors with significant effect on the R-curve-driven parameters (CE, FE and ER) are determined using ANOVA. Subsequently, prediction models are generated based on the effective factors and interactions. Generated models for fracture responses of AC could accurately fit on actual responses with $>0R^2_{adj}$.8, adequate precision greater then 4, and model p-value<0.0001.
- Even though having a lower energy consumption for production and preparation, siliceous aggregate does not exhibit as desirable as limestone in AC mixtures in terms of fracture performance. At low-temperature levels (particularly −20 °C in this research), the cohesive energy, fracture energy, and energy rate magnitudes of the mixtures developed by siliceous aggregate are notably lower than the limestone mixtures.
- Based on the R-curves and the RSM results, it can be concluded that a 20 % crumb rubber modification has significantly improved the fracture performance of the mixtures. In addition to increasing the cohesive energy and the fracture energy of the mixtures at lower temperatures, a desirable increase in the energy rates could be detected. Unmodified mixtures exhibit zero energy rates at −15 °C and below regardless of the aggregate type and size, conducing to entirely unstable crack propagation in the post-peak phase leading to an abrupt failure of the mixture in the AC pavement layer.
- As a result of the multi-objective assessment framework introduced in this research, at a low temperature condition, the environmental index and cost were decreased on average by almost 15 % and 1 % respectively, and fracture responses were enhanced compared to the reference optimal mix design (CRC = 0). Moreover, reduction of the binder content in the optimized mixtures to 4.74 % or 4.77 % by the optimization process is noteworthy in implying the efficiency of the framework.

The well-established assumption of certainty in the objective function coefficients is pursued in this study. In future research, uncertainty analyses can be deemed for solving the optimization problem in order to consider the widely varying performance of asphalt concrete mixtures.

Ethical Statement:

The paper has been submitted with full responsibility, following due ethical procedure, and there is no duplicate publication, fraud, plagiarism. None of the authors of this paper has a financial or personal relationship with other people or organizations that could inappropriately influence or bias the content of the paper.

Funding Body:

There is no Funding support for this research.

CRediT authorship contribution statement

Sepehr Ghafari: Project administration, Supervision, Conceptualization, Data curation, Methodology, Validation, Writing – review & editing. **Sajad Ranjbar:** Methodology, Software, Formal analysis, Visualization, Writing – original draft. **Mehrdad Ehsani:** Methodology, Software, Formal analysis, Visualization. **Fereidoon Moghadas Nejad:** Methodology, Supervision. **Parneet Paul:** .

Declaration of Competing Interest

The authors declare that they have no known competing financial interests or personal relationships that could have appeared to influence the work reported in this paper.

Data availability

Data will be made available on request.

References

[1] E. J. Yoder and M. W. Witczak, *Principles of pavement design*. John Wiley & Sons, 1991.
[2] K.W. Kim, M. El Hussein, Variation of fracture toughness of asphalt concrete under low temperatures, Constr. Build. Mater. 11 (7–8) (1997) 403–411.
[3] M. Eghbali, M.F. Tafti, M. Aliha, H. Motamedi, The effect of ENDB specimen geometry on mode I fracture toughness and fracture energy of HMA and SMA mixtures at low temperatures, Eng. Fract. Mech. 216 (2019), 106496.
[4] A.G. Mahani, P. Bazoobandi, S.M. Hosseinian, H. Ziari, Experimental investigation and multi-objective optimization of fracture properties of asphalt mixtures containing nano-calcium carbonate, Constr. Build. Mater. 285 (2021), 122876.
[5] M.O. Marasteanu, S. Dai, J.F. Labuz, X. Li, Determining the low-temperature fracture toughness of asphalt mixtures, Transp. Res. Rec. 1789 (1) (2002) 191–199.
[6] X. Li, M. Marasteanu, The fracture process zone in asphalt mixture at low temperature, Eng. Fract. Mech. 77 (7) (2010) 1175–1190.
[7] B. Doll, H. Ozer, J. Rivera-Perez, I.L. Al-Qadi, J. Lambros, Damage zone development in heterogeneous asphalt concrete, Eng. Fract. Mech. 182 (2017) 356–371.
[8] M. Aliha, S. Shaker, Effect of bitumen type, temperature and aging on mixed I/II fracture toughness of asphalt binders-experimental and theoretical assessment, Theor. Appl. Fract. Mech. 110 (2020), 102801.
[9] A. Moniri, H. Ziari, A. Amini, M. Hajiloo, Investigating the ANN model for cracking of HMA in terms of temperature, RAP and fibre content, Int. J. Pavement Eng. (2020) 1–13.
[10] J. Stempihar, K. Kaloush, A notched disk crack propagation test for asphalt concrete, MOJ Civil Eng 3 (5) (2017) 00084.
[11] S. Yang, A. Braham, R-curves characterisation analysis for asphalt concrete, Int. J. Pavement Eng. 19 (2) (2018) 99–108.
[12] Y. Zhao, J. Chang, H. Gao, A three-parameter R-curve of concrete-like quasi-brittle materials, Constr. Build. Mater. 78 (2015) 243–249.
[13] X.-K. Zhu, J.A. Joyce, J–Resistance curve testing of HY80 steel using SE (B) specimens and normalization method, Eng. Fract. Mech. 74 (14) (2007) 2263–2281.
[14] K. Ostapska-Luczkowska and K. A. Malo, "Wedge splitting test of wood for fracture parameters estimation of Norway Spruce," 2020.
[15] H. Fischer, W. Rentzsch, R. Marx, R-curve behavior of dental ceramic materials, J. Dent. Res. 81 (8) (2002) 547–551.
[16] S. Ghafari, F.M. Nejad, R-curve behavior and crack propagation properties of asphalt concrete at low temperatures, J. Civ. Eng. Manag. 21 (5) (2015) 559–570.
[17] S. Ghafari, F. Moghadas Nejad, Crack propagation characterization of crumb rubber modified asphalt concrete using J-R curves, Theor. Appl. Fract. Mech. 117 (2022/02/01/ 2022,), 103156, https://doi.org/10.1016/j.tafmec.2021.103156.
[18] S. Yang, A.F. Braham, Influence of binder grade, gradation, temperature and loading rate on R-curve of asphalt concrete, Constr. Build. Mater. 154 (2017) 780–790.
[19] H. Wang, X. Liu, M. van de Ven, G. Lu, S. Erkens, A. Skarpas, Fatigue performance of long-term aged crumb rubber modified bitumen containing warm-mix additives, Constr. Build. Mater. 239 (2020), 117824.
[20] A. Razmi, M. Mirsayar, Fracture resistance of asphalt concrete modified with crumb rubber at low temperatures, Int. J. Pavement Res. Technol. 11 (3) (2018) 265–273.
[21] S. Ghafari, F. Moghadas Nejad, Effect of mode mixity, temperature, binder content, and gradation on mixed mode (I/II) R-curve of asphalt concrete at low temperatures, Constr. Build. Mater. 313 (2021/12/27/ 2021,), 125567, https://doi.org/10.1016/j.conbuildmat.2021.125567.
[22] S. Ghafari and F. Moghadas Nejad, "R-Curve Characterization of Crumb Rubber Modified Asphalt Mixtures Incorporating Warm Mix Additive at Low Temperatures," in *Key Engineering Materials*, 2021, vol. 894: Trans Tech Publ, pp. 109-114.
[23] X. Chen, M. Solaimanian, Evaluating fracture properties of crumb rubber modified asphalt mixes, Int. J. Pavement Res. Technol. 12 (4) (2019) 407–415.
[24] S. Ranjbar, F.M. Nejad, H. Zakeri, An image-based system for pavement crack evaluation using transfer learning and wavelet transform, Int. J. Pavement Res. Technol. 14 (4) (2021) 437–449.
[25] L. F. Facts, "National Asphalt Pavement Association (NAPA), Landham, MD, no date," ed, 2007.
[26] H. Jahanbakhsh, M.M. Karimi, H. Naseri, F.M. Nejad, Sustainable asphalt concrete containing high reclaimed asphalt pavements and recycling agents: Performance assessment, cost analysis, and environmental impact, J. Clean. Prod. 244 (2020), 118837.
[27] C.S. Hanson, R.B. Noland, K.R. Cavale, Life-cycle greenhouse gas emissions of materials used in road construction, Transp. Res. Rec. 2287 (1) (2012) 174–181.
[28] H. Naseri, M. Ehsani, A. Golroo, F. Moghadas Nejad, Sustainable pavement maintenance and rehabilitation planning using differential evolutionary programming and coyote optimisation algorithm, Int. J. Pavement Eng. (2021) 1–18.
[29] R.B. Mallick, A. Veeraragavan, Sustainable pavements in India-the time to start is now, New Building Materials and Construction World (NBM&CW) Magazine 16 (3) (2010) 128–140.
[30] M. Piantanakulchai, H. Inamura, Y. Takeyama, A life cycle inventory analysis of carbon dioxide for a highway construction project using input-output scheme a case study of the Tohoku expressway construction works, Infrastructure Planning Review 16 (1999) 411–418.
[31] F.G. Praticò, M. Giunta, M. Mistretta, T.M. Gulotta, Energy and environmental life cycle assessment of sustainable pavement materials and technologies for urban roads, Sustainability 12 (2) (2020) 704.
[32] M.R. Heidari, G. Heravi, A.N. Esmaeeli, Integrating life-cycle assessment and life-cycle cost analysis to select sustainable pavement: A probabilistic model using managerial flexibilities, J. Clean. Prod. 254 (2020), 120046.
[33] Q.-Z. Wang, N.-N. Wang, M.-L. Tseng, Y.-M. Huang, N.-L. Li, Waste tire recycling assessment: Road application potential and carbon emissions reduction analysis of crumb rubber modified asphalt in China, J. Clean. Prod. 249 (2020), 119411.
[34] M. Fakhri, A. Azami, Evaluation of warm mix asphalt mixtures containing reclaimed asphalt pavement and crumb rubber, J. Clean. Prod. 165 (2017) 1125–1132.
[35] S. Ranjbar, F. M. Nejad, H. Zakeri, and A. H. Gandomi, "3 - Computational intelligence for modeling of asphalt pavement surface distress," in *New Materials in Civil Engineering*, P. Samui, D. Kim, N. R. Iyer, and S. Chaudhary Eds.: Butterworth-Heinemann, 2020, pp. 79-116.
[36] P. Hajikarimi, M. Ehsani, Y.E. Haloui, F.F. Tehrani, J. Absi, F.M. Nejad, Fractional viscoelastic modeling of modified asphalt mastics using response surface method, Constr. Build. Mater. 317 (2022), 125958.
[37] M.J. Nadoushan, P. Dashti, S. Ranjbar, A.A. Ramezanianpour, A. M. Ramezanianpour, R. Banar, RSM-based Optimized Mix Design of Alkali-activated Slag Pastes Based on the Fresh and Hardened Properties and Unit Cost, J. Adv. Concr. Technol. 20 (4) (2022) 300–312, https://doi.org/10.3151/jact.20.300.
[38] S.R. Omranian, M.O. Hamzah, T.S. Yee, M.R. Mohd Hasan, Effects of short-term ageing scenarios on asphalt mixtures' fracture properties using imaging technique and response surface method, Int. J. Pavement Eng. 21 (11) (2020) 1374–1392.
[39] Z.B. Yıldırım, M. Karacasu, Modelling of waste rubber and glass fibber with response surface method in hot mix asphalt, Constr. Build. Mater. 227 (2019/12/10/ 2019,), 117070, https://doi.org/10.1016/j.conbuildmat.2019.117070.
[40] G. Saha, K.P. Biligiri, Cracking performance analysis of asphalt mixtures using response surface methodology: experimental investigations and statistical optimization, Mater. Struct. 50 (1) (2017) 1–12.
[41] W. Rafiq, et al., Modeling and design optimization of reclaimed asphalt pavement containing crude palm oil using response surface methodology, Constr. Build. Mater. 291 (2021), 123288.
[42] L.-J. Chai, et al., Fracture mechanics-based mixture optimization of ecological high-ductility cementitious composites modified with recycled asphalt concrete, Constr. Build. Mater. 264 (2020), 120686.
[43] M. Pszczoła, M. Jaczewski, C. Szydłowski, J. Judycki, B. Dołżycki, Evaluation of low temperature properties of rubberized asphalt mixtures, Procedia Eng. 172 (2017) 897–904.
[44] P.S. Wulandari, D. Tjandra, Use of crumb rubber as an additive in asphalt concrete mixture, Procedia Eng. 171 (2017) 1384–1389.
[45] F. Farshidi, D. Jones, and J. T. Harvey, "Warm-Mix Asphalt Study: Evaluation of Rubberized Hot-and Warm-Mix Asphalt with Respect to Emissions," 2013.
[46] G.L. Baumgardner, G.R. Reinke, Binder additives for warm mix asphalt technology, J. Assoc. Asphalt Paving Technol. no. 82 (2013).
[47] M. P. Wagoner, W. G. Buttlar, and G. H. Paulino, "Development of a single-edge notched beam test for the study of asphalt concrete fracture," in *Advances in Pavement Engineering*, 2005, pp. 1-13.
[48] M.P. Wagoner, W.G. Buttlar, G.H. Paulino, Development of a single-edge notched beam test for asphalt concrete mixtures, J. Test. Eval. 33 (6) (2005) 452–460.
[49] S. Ghafari, M. Ehsani, F.M. Nejad, Prediction of low-temperature fracture resistance curves of unmodified and crumb rubber modified hot mix asphalt mixtures using a machine learning approach, Constr. Build. Mater. 314 (2022), 125332.
[50] T. L. Anderson, *Fracture mechanics: fundamentals and applications*. CRC press, 2017.
[51] S. Kittipongvises, Assessment of Environmental Impacts of Limestone Quarrying Operations in Thailand, Environmental & Climate Technologies 20 (1) (2017) pp.

[52] A. Farina, M.C. Zanetti, E. Santagata, G.A. Blengini, Life cycle assessment applied to bituminous mixtures containing recycled materials: Crumb rubber and reclaimed asphalt pavement, Resour. Conserv. Recycl. 117 (2017) 204–212.
[53] M. Ehsani, F. Moghadas Nejad, P. Hajikarimi, Developing an optimized faulting prediction model in Jointed Plain Concrete Pavement using artificial neural networks and random forest methods, Int. J. Pavement Eng. (2022) 1–16, https://doi.org/10.1080/10298436.2022.2057975.
[54] Z. Mao, "Life-Cycle Assessment of Highway Pavement Alternatives in Aspects of Economic, Environmental, and Social Performance," Texas A & M University, 2012.
[55] S. Bhattacharya, "Central composite design for response surface methodology and its application in pharmacy," in *Response Surface Methodology in Engineering Science*: IntechOpen, 2021.
[56] B. Ait-Amir, P. Pougnet, and A. El Hami, "6 - Meta-Model Development," in *Embedded Mechatronic Systems 2*, A. El Hami and P. Pougnet Eds.: Elsevier, 2015, pp. 151-179.
[57] N. Bala, M. Napiah, I. Kamaruddin, Nanosilica composite asphalt mixtures performance-based design and optimisation using response surface methodology, Int. J. Pavement Eng. 21 (1) (2020) 29–40.
[58] T.O. Okyay, D.F. Rodrigues, Optimized carbonate micro-particle production by Sporosarcina pasteurii using response surface methodology, Ecol. Eng. 62 (2014) 168–174.
[59] M. Kahani, F. Kalantary, M.R. Soudi, L. Pakdel, S. Aghaalizadeh, Optimization of cost effective culture medium for Sporosarcina pasteurii as biocementing agent using response surface methodology: Up cycling dairy waste and seawater, J. Clean. Prod. 253 (2020), 120022.
[60] A. Cuadri, P. Partal, N. Ahmad, J. Grenfell, G. Airey, Chemically modified bitumens with enhanced rheology and adhesion properties to siliceous aggregates, Constr. Build. Mater. 93 (2015) 766–774.
[61] M.A. Abdelrahman, S.H. Carpenter, Mechanism of interaction of asphalt cement with crumb rubber modifier, Transp. Res. Rec. 1661 (1) (1999) 106–113.
[62] A. Ghavibazoo, M. Abdelrahman, Composition analysis of crumb rubber during interaction with asphalt and effect on properties of binder, Int. J. Pavement Eng. 14 (5) (2013) 517–530.
[63] A. Danesh, M. Ehsani, F. Moghadas Nejad, H. Zakeri, Prediction model of crash severity in imbalanced dataset using data leveling methods and metaheuristic optimization algorithms, Int. J. Crashworthiness (2022) 1–14.
[64] M.G. Zamani, A. Moridi, J. Yazdi, Groundwater management in arid and semi-arid regions, Arab. J. Geosci. 15 (4) (2022) 1–14.